Carbohydrate Polymers 82 (2010) 942–951

Contents lists available at ScienceDirect

Carbohydrate Polymers

journal homepage: www.elsevier.com/locate/carbpol

Preparation, characterization and evaluation of selenite-loaded chitosan/TPP nanoparticles with or without zein coating

Yangchao Luo, Boce Zhang, Wen-Hsing Cheng, Qin Wang*

Department of Nutrition and Food Science, University of Maryland, 0112 Skinner Building, College Park, MD 20742, United States

ARTICLE INFO

Article history:
Received 29 May 2010
Received in revised form 7 June 2010
Accepted 11 June 2010
Available online 25 June 2010

Keywords:
Chitosan
Zein
Selenite
Nanoparticles
Controlled release

ABSTRACT

The selenite-loaded chitosan (CS) nanoparticles using tripolyphosphate (TPP) as a cross-linking agent with or without zein (a water insoluble corn protein) coating were prepared to obtain selenite supplement formulations with low toxicity and improved antioxidant property. Scanning electron microscopy observation showed selenite-loaded CS/TPP nanoparticles had a spherical shape with uniform diameter (100–300 nm). The results demonstrated that particle size, surface charge, encapsulation efficiency, and release profile could be modulated by fabricating conditions. After coated with zein, the particle size maintained nanoscale (200–400 nm) while encapsulation efficiency increased from 60% to 95%. The release profile was also prominently improved with zein coating, the released selenite reduced from 85% to 30% within 4 h in PBS. In simulated gastrointestinal condition with enzymes, 93% of selenite released from non-coated CS/TPP nanoparticles into gastric fluid, however, the releasing rate decreased to 46% after coated with zein. Moreover, due to high antioxidant activity of CS, the *in vitro* antioxidant properties of selenite-loaded CS/TPP nanoparticles were significantly enhanced, compared with pure selenite.

1. Introduction

Selenium is an essential trace element in human nutrition closely associated with the population health. It plays an important role to prevent various diseases, such as hypercholesterolemia (Navas-Acien, Bley, & Guallar, 2008), cardiovascular disease (Ray et al., 2006; Thomson, 2004), and certain cancers (Ferguson, Philpott, & Karunasinghe, 2006). Although food and vegetables can be the major source of selenium intake, selenium supplementation is still needed in the low selenium areas (Navarro-Alarcon & Cabrera-Vique, 2008). Available dietary supplement of selenium mainly consists of two inorganic forms, selenite and selenate, both of them are considered toxic if consumed in large quantity. Sodium selenite has been used in the selenium-fortified milk formula, especially for infants, however, many studies reported that 50–90% of consumed selenite was lost and excreted in urine due to the short retention time in gastrointestinal tract (Dael, Davidsson, Munoz-Box, Fay, & Barclay, 2001; Zachara, Gromadzinska, Wasowizc, & Zbrog, 2006). It has been also evidenced that supplementation of selenite to mice and cells may cause various adverse effects due to its pro-oxidant property, which depends on the concentration and other factors (Björkhem-Bergman et al., 2002; Cheng, 2009; Moak & Christensen, 2001; Shimizu, Ueno, Okuno, Sakazaki, & Nakamuro, 2009; Xiang, Zhao, & Zhong, 2009). Therefore, how to provide efficient and safe application of dietary selenite supplementation has become a challenge topic in recent years.

Chitosan (CS), the *N-deacetylation* form of chitin mostly found in the exoskeleton of crustacean, insects, and fungi, is a natural polysaccharide. CS is not only non-toxic and biodegradable with low immunogenicity, but also possesses a high density of positive charge in an acid solution attributed to the glucosamine group on its backbone. Because of these beneficial characteristics, increasing attention has been drawn to the applications of CS-based micro- and nanoparticles in the pharmaceutical and nutraceutical field (Grenha, Seijo, & Remuñán-López, 2005; Khlifi, EI Hachimi, Khalil, Es-Safi, & EI Abbouyi, 2005; Kockisch, Ress, Young, Tsibouklis, & Smart, 2003; Shah, Pal, Kaushik, & Devi, 2009). Ionic gelation is the most studied and widely used method for fabricating CS nanoparticles, in which cationic CS and multivalent polyanions interact to form CS nanoparticles under simple and mild conditions. Among various polyanions, tripolyphosphate (TPP) is the most investigated due to its quick gelling capability and non-toxic property. CS/TPP nanoparticles have been proved to be excellent carriers for drug and nutrient in therapeutic and nutritional applications, such as providing efficient and target delivery of shRNA sequence (Wang et al., 2009), lowering toxicity of therapeutic antisense oligonucleiotide (Dung et al., 2007), increasing bioavailability of nutraceuticals (Dudhani & Kosaraju, 2010; Hu et al., 2008; Zhang, Yang, Tang, Hu, & Zou, 2008), as well as achieving long term controlled release of protein, e.g., bovine serum albumin (Gan & Wang,

* Corresponding author. Tel.: +1 301 405 8421; fax: +1 301 314 3313.
E-mail address: wangqin@umd.edu (Q. Wang).

0144-8617/$ – see front matter © 2010 Elsevier Ltd. All rights reserved.
doi:10.1016/j.carbpol.2010.06.029

2007) and unstable drugs, e.g., venlafaxin hydrochloride (Shah et al., 2009).

In the last decade, CS has already been introduced to decrease toxic effects and enhance beneficial properties of therapeutic treatment of selenium compounds. CS hydrogen selenite was prepared by the reaction between CS and selenous acid (Qin, Xiao, Du, & Gao, 2002). It was found that CS hydrogen selenite inhibited the growth against sarcoma 180 solid tumor cells with lower acute toxicity, comparing to sodium selenite. Seleno-short chain CS is a newly developed CS derivative modified by introducing selenic acid groups ($-SeO_3$) to amino positions of CS (Patent Number CN1600793A), and proved to possess a therapeutic potential in human treatment with improved efficacy (Liu, Song, Cao, Liu, & Jia, 2008).

In this study, CS/TPP was chosen to form nanoparticles with sodium selenite to decrease the toxicity (personal communication with Dr. Wen-Hsing Cheng) and enhance the antioxidant property of selenite dietary supplement. The ionic gelation method was used to prepare CS/TPP nanoparticles to encapsulate sodium selenite. Different fabricating conditions were evaluated in terms of their effects on physicochemical properties of selenite-loaded CS/TPP nanoparticles, including morphology, particles size, surface charge, the encapsulation efficiency, and release profile, as well as the antioxidant properties. Furthermore, zein, a water insoluble corn protein, was chosen as a coating material to achieve better encapsulation efficiency and controlled release profiles of selenite-loaded CS/TPP nanoparticles.

2. Materials and methods

2.1. Materials

Low molecular weight CS with 92% deacytelation degree (Batch No.: MKBB4232), TPP, sodium selenite, 2,3-diaminonaphthalene (DAN), linoleic acid, 1,10-phenanthroline, and pepsin were purchased from Sigma–Aldrich Chemical Co. Ltd. (St. Louis, MO). Disodium salt of ethylenediaminetetraacetic acid (EDTA) solution (5 M) was obtained from Boston Bioproducts Incorporation (Boston, MA). Phosphate butter saline (PBS) was purchased from EMD Chemicals Incorporation (Gibbstown, NJ). Simulated gastric fluid without pepsin (SGF) and simulated intestinal fluid with pancreatin (SIF) were purchased from RICCA Chemical Company (Arlington, TX). Zein sample with a minimum protein content of 97% was provided by Showa Sangyo (Tokyo, Japan). All other reagents, including $FeSO_4$ and H_2O_2, were of analytical grade. DAN was dissolved in 0.1 M hydrochloric acid to prepare a 0.1% solution; once dissolved, it was extracted with cyclohexane three times to remove impurities.

2.2. Preparation of selenite-loaded CS/TPP nanoparticles

CS solution (5 mg/ml) was prepared by dissolving CS in 1% (w/v) acetic acid solution under stirring overnight at room temperature. The CS solution was diluted with deionized water (refer to water thereafter) to produce different concentrations. CS/TPP nanoparticles were prepared according to the ionotropic gelation process. In brief, TPP aqueous solution (0.5 mg/ml) was added dropwise to the CS solution and stirred (600 rpm) for 30 min at room temperature to obtain blank nanoparticles. For preparation of selenite-loaded CS/TPP nanoparticles, the selenite solution with various concentrations was added slowly to CS solution with mild stirring (600 rpm) for 30 min at room temperature, and then TPP solution was added dropwise to the mixture with mild stirring (600 rpm) for another 30 min. The CS/TPP weight ratio used throughout this study was 5:1, which was obtained from the results of several trials.

2.3. Fourier transform infrared spectroscopy (FTIR)

FTIR was used to measure changes in chemical structure of the CS, blank nanoparticles, and selenite-loaded nanoparticle samples. The samples were first lyophilized (RVT 4104-115, Refrigerated Vapor Trap, Thermo Savant, Waltham, MA), and then ground into homogeneous powders. The spectra were acquired at 600–4000 cm^{-1} wavenumbers with a 4 cm^{-1} resolution utilizing a NEXUS 670 FTIR spectrophotometer (Thermo Nicolet Corp., Madison, WI) equipped with a diamond ATR cell.

2.4. Morphology observation

Morphological structures of TPP, selenite, CS, CS/TPP, selenite-loaded CS/TPP nanoparticles, and zein-coated nanoparticles were obtained by a scanning electron microscopy (SEM, Hitachi SU-70 Pleasanton, CA). Samples were first cast-dried on an aluminum pan before cutting into an appropriate size, and then adhered to conductive carbon tapes (Electron Microscopy Sciences, Ft. Washington, PA). Subsequently, they were mounted on specimen stubs, and coated with a thin (<20 nm) conductive gold and platinum layer using a sputter coater (Hummer XP, Anatech, CA). Representative SEM images were reported in Section 3.

2.5. Measurement of particle size and surface charge

Hydrodynamic diameter of selenite-loaded CS/TPP nanoparticles was measured by a dynamic light scattering instrument (DLS, BI-200SM, Brookhaven Instruments Corp., Holtsville, NY). DLS is equipped with a 35 mW HeNe laser beam at a wavelength of 637 nm. All DLS measurements were performed at 25 °C. Reflective index and viscosity of water were 1.590 and 0.8904 cP, respectively, which were used for calculating effective diameter from autocorrelation. Surface charges of the nanoparticles were measured by a laser Doppler velocimetry (Zetasizer Nano ZS90, Malvern, UK), using a fold capillary cuvette (Folded Capillary Cell-DTS1060, Malvern, UK). The freshly prepared solutions of nanoparticles were used for particle size and surface charge measurement. All measurements were conducted in triplicate.

2.6. Encapsulation efficiency of nanoparticles

The encapsulation efficiency (EE) of the nanoparticles was defined as the drug content that is entrapped into nanoparticles (Hu et al., 2008; Shah et al., 2009), and calculated as follows:

$$\mathrm{EE}\,(\%) = \frac{\text{Total selenite amount} - \text{Free selenite amount}}{\text{Total selenite amount}} \times 100$$

The total selenite amount was the added selenite. Amount of free selenite molecules were obtained using a membrane separation method. First, free selenite was separated from nanoparticles using an Ultra-15 centrifugal filter device (Millipore Corp., Ann Arbor, MI) with 10 kDa molecular weight cut off, according to the previously reported method (Hu et al., 2008). Being centrifuged at 4000 × *g* for 30 min, free selenite molecules would penetrate into the filtrate receiver, and the CS nanoparticles would stay in the filter unit. The separated nanoparticles were then lyophilized for further characterization. The free selenite content in the filtrate was measured using the method of Veiga, Rivero-Huguet, and Huertas (2008) with modifications. In brief, nanoparticles solution was appropriately diluted with water, and then 5 ml sample solution was poured into a test tube, followed by adding 2 ml 0.05 M EDTA and 2 ml 0.1% DAN solution. The tubes were warmed at 60 °C for 30 min. The formed piaselenol was extracted by 4 ml cyclohexane. The absorbance in the cyclohexane layer was measured at 378 nm by a spectrophotometer (Beckman Coulter, DU-730, Fullerton, CA). The amount of

selenite was calculated by appropriate calibration curve of free selenite (R^2 = 0.9979), and each measurement was conducted in triplicate. And the content of selenite entrapped in the CS/TPP matrix was measured right after the separation using the same method to confirm that the addition of free selenite and encapsulated selenite equaled to the total content of added selenite.

2.7. In vitro release of selenite from nanoparticles

In vitro release study of selenite from nanoparticles was carried out in PBS medium, according to a reported procedure (Shah et al., 2009). Certain amount (5–10 mg) of nanoparticles were resuspended in PBS with pH 7.4 and placed in a dialysis membrane bag with molecular weight cut off at 10 kDa. The membrane bag was placed in 50 ml PBS. The entire system was then kept at 37 °C with mild and continuous stirring. At certain time intervals, 5 ml release medium was collected and 5 ml fresh PBS was replaced into release system. The release of selenite from nanoparticles was also investigated under simulated gastrointestinal tract (GI tract), according to the reported method (Somchue, Sermsri, Shiowatana, & Siripinyanond, 2009). The nanoparticles with or without coating were first incubated in 10 ml of SGF with 0.1% pepsin (w/v) at 37 °C under mild stirring for 2 h. The supernatant was separated by centrifugation for determination of selenite content. The swollen aggregates were collected and subsequently incubated in SIF with 1.0% pancreatin (w/v) at 37 °C under mild stirring for 4 h. The supernatant was separated by centrifugation for determination of selenite content. The content of selenite was measured by the method described in Section 2.6.

2.8. Antioxidative properties of nanoparticles

Two methods, hydroxyl radical scavenging effect and inhibitory effect against lipid peroxidation, were used to evaluate the antioxidant properties of selenite and selenite-loaded CS/TPP nanoparticles.

2.8.1. Hydroxyl radical scavenging effect (HRSE)

The hydroxyl radical scavenging experiment was carried out using the method described by Tian et al. (2009) with some modifications. In brief, 1,10-phenanthroline (1 ml, 0.93 mM), the selenite, CS, or selenite-loaded nanoparticles sample (1 ml), and an acetate buffer (1 ml, 0.3 M, pH = 3.6) were added to a screw-capped tube orderly and mixed thoroughly. Then, $FeSO_4{\cdot}7H_2O$ (1 ml, 0.93 mM) was pipetted to the mixture. The reaction was initiated by adding H_2O_2 (1 ml, 0.025%, v/v). The mixture was incubated at 37 °C for 60 min, and the absorbance was measured at 509 nm against reagent blank. The negative control was prepared by replacing 1 ml sample with water, and the blank control was prepared by replacing 1 ml H_2O_2 with 1 ml water. The HRSE was calculated using the following formula:

$$\mathrm{HRSE}\,(\%) = \frac{A_s - A_n}{A_b - A_n} \times 100$$

where A_s, A_n and A_b were the absorbance values of the sample, negative control, and blank control, respectively. Determination of each sample was performed in triplicate.

2.8.2. Inhibitory effect against lipid peroxidation (IEALP)

The inhibitory effect of selenite, CS, and selenite-loaded nanoparticles against lipid peroxidation was evaluated by the formation of conjugated dienes in linoleic acid emulsion system, according to the procedure prescribed by Khlifi et al. (2005), with minor modification. In brief, a 100 μl sample was added to 2.0 ml of 10 mM linoleic acid in phosphate buffer (pH 7.0, 10 mM) emulsified with Tween 20. The mixture was incubated in darkness at 37 °C to accelerate oxidation. The control was prepared by replacing 100 μl sample with 100 μl water. After incubation for 15 h, the absorbance was measured at 234 nm against reagent blank. The IEALP was calculated with the following equation:

$$\mathrm{IEALP}\,(\%) = \frac{A_c - A_s}{A_c} \times 100$$

where A_c and A_s were the absorbance of the control and sample, respectively.

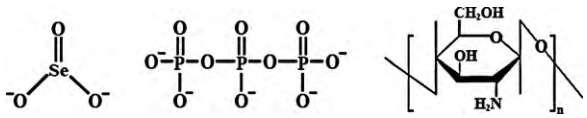

Fig. 1. Molecular structure of selenite, TPP and CS.

2.9. Improved nanoparticle formulation with zein coating

To prepare zein-coated selenite-loaded CS/TPP nanoparticles, the selenite-loaded CS/TPP nanoparticles was first prepared (CS concentration, 1.5 mg/ml; selenite loading concentration, 0.6 mg/ml) and then mixed with proper volume of ethanol. Then, the appropriate concentration of zein was dropwise added to above solution under mild stirring for 30 min. The mass ratio of CS to zein was 1:1 and 1:3. The particle size, encapsulation efficiency and release profile were further evaluated and compared with nanoparticles without zein coating.

2.10. Statistical analysis

All the experiments were conducted in triplicate with data reported as mean ± standard error. Experimental statistics were performed using the SAS software (Version 9.2, SAS Institute Inc., Cary, NC). The Student's *t*-test was used to compare the treatment means of antioxidant activities between nanoparticles and selenite or CS. The analysis of variance (ANOVA) Tukey's multiple comparison tests was used in analysis of differences between physicochemical properties of nanoparticles with and without zein coating. The significance level (P) was set at 0.05.

3. Results and discussion

3.1. Physicochemical characterization

The molecular structures of selenite, TPP, and CS are shown in Fig. 1. CS is a cationic polyelectrolyte polysaccharide due to the protonation of amino groups in acidic solution. Each selenite and TPP molecule carries a maximum of two and five negative charges, respectively.

3.1.1. FTIR results

The intermolecular interaction of nanoparticles was characterized by FTIR (Fig. 2). Six characterization peaks, observed in CS (Fig. 2A) at 3358.52, 1648.61, 1586.59, 1418.88, 1375.24, and 1025.94 cm^{-1}, were thought to be O–H stretch, C=O stretching from amide I, N–H bending and C–N stretching from amide II, $-CH_2$ bending, $-CH_3$ symmetrical deformation, and skeletal vibration of C–O stretching, respectively (Lawrie et al., 2007; Shah et al., 2009). It was observed that the spectrum of CS/TPP nanoparticles was different from that of CS matrix (Fig. 2B), highlighted in the wavenumber range from 1500 to 3500 cm^{-1}. The peak of 3358.52 cm^{-1} became wider and flatter, indicating that hydrogen bonding was enhanced (Wu, Yang, Wang, Hu, & Fu, 2005). The peaks of amide I and amide II in CS/TPP nanoparticles shifted to 1635.52 and 1558.23 cm^{-1},

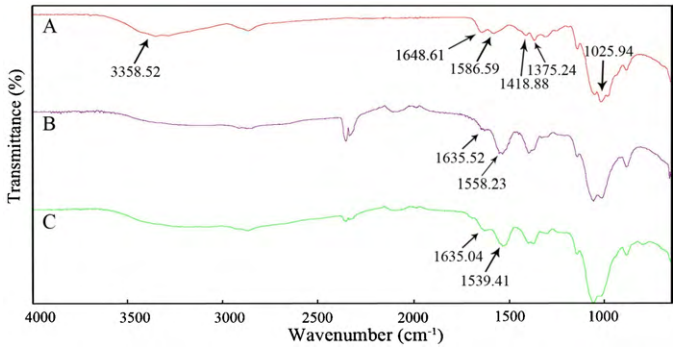

Fig. 2. FTIR spectra of CS (A), CS/TPP nanoparticles (B) and selenite-CS/TPP nanoparticles (C).

respectively, due to the electrostatic interaction between phosphoric groups of TPP and amino groups of CS in nanoparticles. These observations were consistent with the results reported previously (Hu et al., 2008; Shah et al., 2009; Wu et al., 2005). Compared with the spectrum of CS/TPP nanoparticles, the electrostatic interaction between selenite and amino groups was confirmed by the shift of absorption peaks of amide II from 1558.23 to 1539.41 in the spectrum of selenite-loaded CS/TPP nanoparticles (Fig. 2C). This phenomenon was further confirmed by surface charge results presented in Section 3.3.

3.1.2. Morphological observation

The morphological changes of each ingredient and nanoparticles after cast drying on an aluminum surface were observed with a SEM, as shown in Fig. 3. Positively charged pure CS exhibited rough membrane structures (Fig. 3A) due to its ability to form films by cast drying (Picker-Freyer & Brink, 2006), while the negatively charged TPP formed smooth film (Fig. 3B). As an inorganic molecule, sodium selenite crystallized into a needle-shaped structure with a diameter of 1–2 μm (Fig. 3C). When mixing CS and TPP together with or without selenite, spherical particles with uniform particle size in the nanoscale formed, ranging from 200 to 300 nm (Fig. 3D and E). The rod shape aggregates, as observed in the SEM photos probably formed during the drying process. The particle size of nanoparticles obtained after cast drying was in good agreement with that measured in an acidic aqueous system presented in the next section.

3.2. Effect of different formulations on particle size

The effects of CS concentration and selenite loading concentration on particle size and polydispersity index (PDI) of selenite-loaded CS/TPP nanoparticles were summarized in Table 1. The particle size increased linearly from 120 to 300 nm with the increase of CS concentration in the range of 0.5–2.5 mg/ml (R^2 = 0.9528). These trends were in accordance with previously reported results (Gan, Wang, Cochrane, & McCarron, 2005; Hu et al., 2008). However, when the selenite concentration increased from 0.2 to 1.0 mg/ml, the particle size decreased slightly from 300 to 200 nm, showing a linearly negative correlation between selenite loading concentration and CS concentration (R^2 = 0.9597). This result is expected since selenite carried negative charges and electrostatically interacted with CS, which would promote formation of nanoparticles through ionic cross-linking. All formulations of selenite-loaded nanoparticles had a small PDI, and increased slightly with increasing of chitosan concentrations (Table 1).

Particle size is one of the most important parameters determining biocompatibilities and bioactivities of micro- and nanoparticles. Small nanoparticles have a higher intracellular uptake than large ones. Desai, Labhasetwar, Amidon, and Levy (1996) reported that the gastrointestinal uptake of particles of 100 nm was 15–250 fold greater than larger size microparticles. In another study, they also pointed out that the uptake mechanism of biodegradable microparticles in Caco-2 cells was largely dependent on particle sizes, as the cell uptakes of particles with 100 nm diameter was 2.5 and 6 times greater than those with 1 μm and 10 μm, respectively (Desai, Labhasetwar, Walter, Levy, & Amidon, 1997). Since particle size plays a vital role in mucosal and epithelial tissue uptake and intracellular trafficking of nanoparticles (Gan et al., 2005), it is possible to enhance the mucoadhesive properties of CS nanoparticles by decreasing its particle size, and thus to improve mucosal uptake of selenium from selenite-loaded nanoparticles.

3.3. Effect of different formulations on surface charge

As soon as CS and TPP were mixed together in an acetic acid, the nanoparticles were formed spontaneously with a significant positive surface charge obtained by the zeta potential measurement (37–50 mV, Fig. 4). Since CS/TPP nanoparticles were formed by the interaction between protonized $-NH_3^+$ in CS and the polyanionic phosphate groups in TPP, the zeta potential of nanoparticles increased linearly due to a more available protonized $-NH_3^+$ on the surface of nanoparticles formed with higher CS concentration (Fig. 4A). However, zeta potential decreased slightly with the increase of selenite concentration (Fig. 4B), owing to an electrostatic interaction between protonized $-NH_3^+$ of CS and selenite that resulted in reduced surface charge.

Zeta potential is another key parameters contributing to various nutritional properties of CS nanoparticles. It has been well documented that CS possesses mucoadhesive properties (Kockisch et al., 2003; Shimoda, Onishi, & Machida, 2001; Sinha, Singla, Wadlhawan, Kaushik, & Kumria, 2004) due to molecular attractive forces formed by an electrostatic interaction between positively charged CS and negatively charged mucosal surfaces. Since most tumor cell membranes are negatively charged, CS nanoparticles have recently been studied to develop tumor-specific delivery of anticancer drugs. For example, encapsulation of paclitaxel using CS-modified nanoparticles could significantly increase lung tumor-specific distribution and enhance the uptake across the endothelial cells of the lung tumor capillary (Yang et al., 2009). Thus, it is pos-

Table 1
The particle size and PDI of different formulations.

Nanoparticles	Particle size	PDI	Nanoparticles	Particle size	PDI
A1	124.27 ± 4.39	0.16 ± 0.03	B1	302.63 ± 6.23	0.21 ± 0.05
A2	203.53 ± 4.93	0.18 ± 0.03	B2	276.00 ± 4.5	0.19 ± 0.05
A3	233.05 ± 9.86	0.18 ± 0.03	B3	233.05 ± 9.86	0.18 ± 0.03
A4	254.55 ± 9.67	0.29 ± 0.01	B4	229.20 ± 5.31	0.23 ± 0.02
A5	304.20 ± 9.11	0.28 ± 0.01	B5	214.43 ± 11.64	0.28 ± 0.01

PDI, polydispersity index. A1, A2, A3, A4 and A5 were the nanoparticle samples with CS concentrations of 0.5, 1.0, 1.5, 2.0, and 2.5 mg/ml, respectively, while the selenite loading concentration and CS-TPP mass ratio were fixed at 0.6 mg/ml and 5:1, respectively. B1, B2, B3, B4, and B5 were the nanoparticles samples with selenite loading concentrations of 0.2, 0.4, 0.6, 0.8, and 1.0 mg/ml, respectively, while the CS concentration and CS-TPP mass ratio were fixed at 1.5 mg/ml and 5:1, respectively. Values were expressed as mean ± standard error.

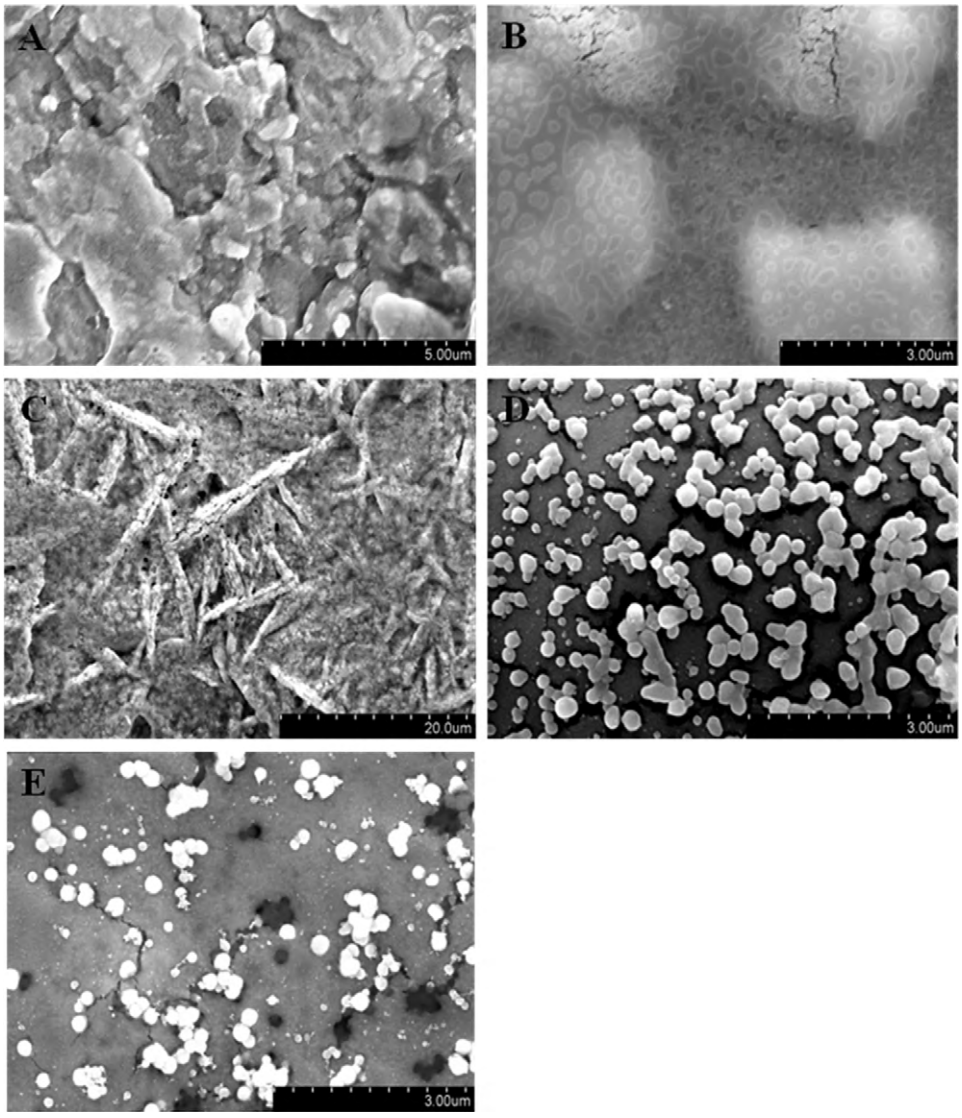

Fig. 3. Scanning electron microscopy (SEM) photographs of CS (A), TPP (B), selenite (C), CS/TPP nanoparticles (D), and selenite-loaded CS/TPP nanoparticles (E).

sible that encapsulation of selenite into CS/TPP nanoparticles may contribute to the increased efficiency of targeted delivery to tumors and lower its toxicity to normal cells and tissues.

3.4. Effect of different formulations on encapsulation efficiency

Encapsulation efficiency is defined as percentage of selenite loading content that can be entrapped into CS/TPP nanoparticles. The effects of CS concentration and selenite loading concentration on encapsulation efficiency were demonstrated in Fig. 4A and B, respectively. With the increase of initial CS concentration during the encapsulation process, more protonized CS ($-NH_3^+$) were available in the system, evidenced by increased surface charge, leading to a stronger electrostatic attraction between selenite and CS. Thus, the encapsulation efficiency of selenite increased linearly with the increase of CS concentration (Fig. 4A). This observation was accordance with the previous studies, showing the encapsulation efficiency of catechins was positively associated with CS initial concentration (Hu et al., 2008). As shown in Fig. 4B, encapsulation efficiency was affected by the initial loading concentration of selenite in a CS solution. A dramatic decrease of encapsulation efficiency from 85% to 42% was observed when loading concentration of selenite increased from 0.2 to 1.0 mg/ml. A reversed linear correlation was obtained between encapsulation efficiency and selenite loading concentration. As the selenite loading concentration increased, more selenite molecules were just electrostatically adsorbed onto the surface of CS and were easily separated from CS nanoparticles by centrifugation. Similar results were also reported by Wu et al. (2005) showing that encapsulation efficiency of ammonium glycyrrhizinate in CS/TPP nanoparticles decreased with increasing drug loading concentration.

3.5. Effect of different formulations on release profile

Fig. 5 presented the *in vitro* release profiles of selenite from CS/TPP nanoparticles, with respect to different CS concentration (Fig. 5A) and different selenite loading concentration (Fig. 5B). Analyses of selenite release showed a very rapid initial burst (0–60 min), followed by a very slow release in all samples. Accumulative release at 240 min was reduced from 98% to 85% with CS concentration increased from 0.5 to 2.5 mg/ml, and the initial burst effect also reduced slightly. These results indicated that the higher the CS concentration was the lower the release rate would be (Fig. 5A). Similar results were also reported in other studies (Hu et al., 2008; Ko,

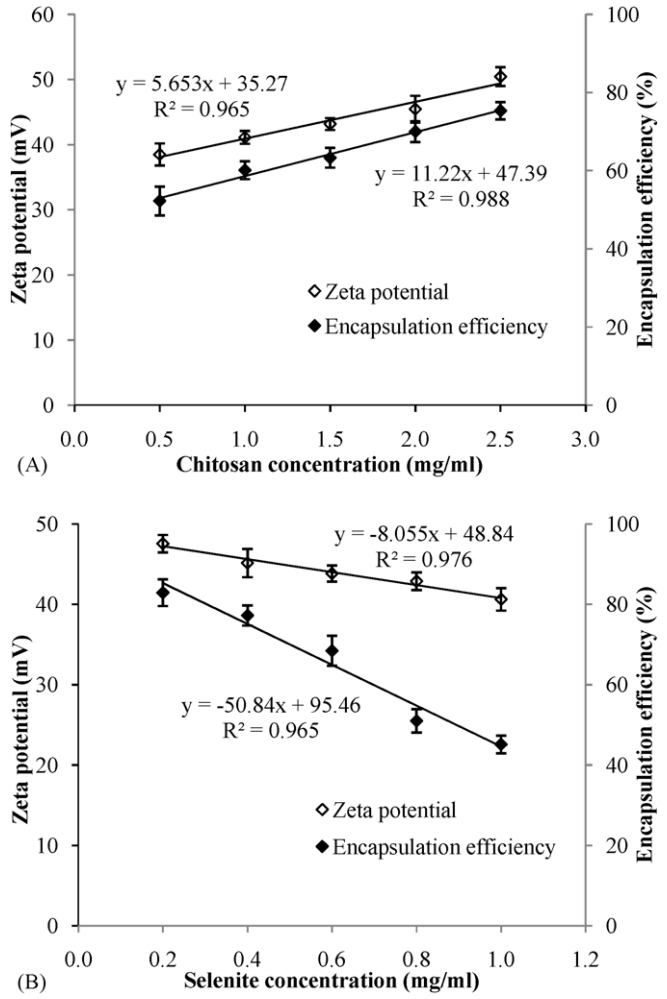

Fig. 4. (A) Effect of CS concentrations on zeta potential and encapsulation efficiency of selenite-loaded CS/TPP nanoparticles (selenite loading concentration = 0.6 mg/ml, CS-TPP mass ratio = 5:1). (B) Effect of selenite loading concentration on zeta potential and encapsulation efficiency of selenite-loaded CS/TPP nanoparticles (CS concentration = 1.5 mg/ml, CS-TPP mass ratio = 5:1). Values were expressed as mean ± standard error.

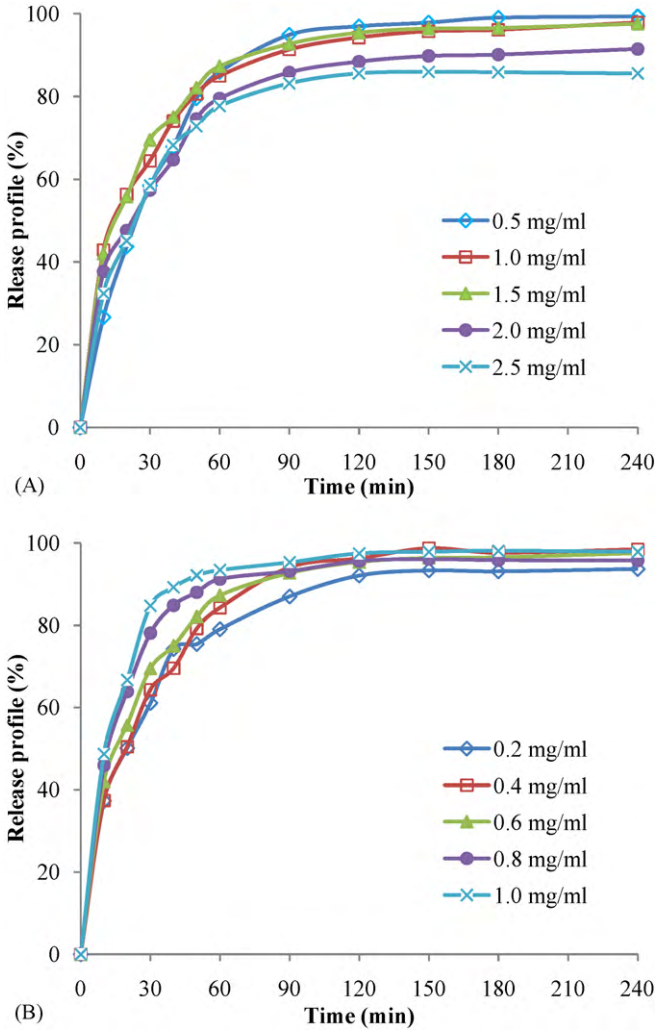

Fig. 5. (A) Effect of CS concentrations on release profile of selenite-loaded CS/TPP nanoparticles (selenite loading concentration = 0.6 mg/ml, CS-TPP mass ratio = 5:1). (B) Effect of selenite loading concentrations on release profile of selenite-loaded CS/TPP nanoparticles (CS concentration = 1.5 mg/ml, CS-TPP mass ratio = 5:1). Values were expressed as mean ± standard error.

Park, Hwang, Park, & Lee, 2002). This phenomenon was attributed to that the increased viscosity at higher CS concentration would result in formation of the denser selenite-loaded CS particles upon interaction with TPP, and thus the greater cross-linking density and less swelling ability (Shah et al., 2009). In addition, increasing CS concentration would lower the membrane permeability of CS nanoparticles, leading to increased chain packing and rigidity, as well as interchain bonding.

Selenite release from the nanoparticles was also dependent on selenite loading concentration (Fig. 5B). As the selenite loading concentration increased from 0.2 to 1.0 mg/ml, greater initial burst effect was observed at higher selenite loading concentration. Almost 85% selenite was released from nanoparticles at 1.0 mg/ml selenite loading concentration within 30 min, whereas the amount of selenite released from nanoparticles decreased to 60% when 0.2 mg/ml selenite loading concentration was used.

Drug molecules diffusion and polymer matrix degradation have been suggested as mechanisms of release profile from nanoparticles and microspheres (Zhou, Deng, & Li, 2001). By studying ammonium glycyrrhizinate loaded CS nanoparticles, Wu et al. (2005) proposed that drug molecule diffusion played a predominant role in release profile when the size of encapsulated drug molecule was much smaller than the formed nanoparticles. Thus, as demonstrated by the release profiles, due to the much smaller size of selenite used in this study, the selenite could diffuse very easily through the surface or the pore of nanoparticles in a very short period of time. Since the formulated selenite-loaded CS/TPP nanoparticles had fast releasing property that is hard to achieve the controlled release purpose, zein was further formulated as a hydrophobic material to coat the nanoparticles to obtain better encapsulation efficiency and release profile and the results were presented in Section 3.7.

3.6. Evaluation of antioxidative properties of selenite-loaded CS/TPP nanoparticles

3.6.1. Hydroxyl radical scavenging effect (HRSE)

Results presented in Fig. 6 demonstrated the scavenging effect of selenite-loaded nanoparticles, CS (Fig. 6A) and selenite (Fig. 6B) on hydroxyl radicals. From Fig. 6A, it was observed that HRSE of nanoparticles increased from 34.1% to 42.5% as the CS concentration increased from 0.5 to 2.5 mg/ml, and that there was no significant difference between HRSE of CS and that of selenite-loaded CS nanoparticles at higher CS concentrations. From Fig. 6B, it was found that HRSE of nanoparticles was also slightly enhanced with an increase in selenite loading concentration. However, the HRSE of

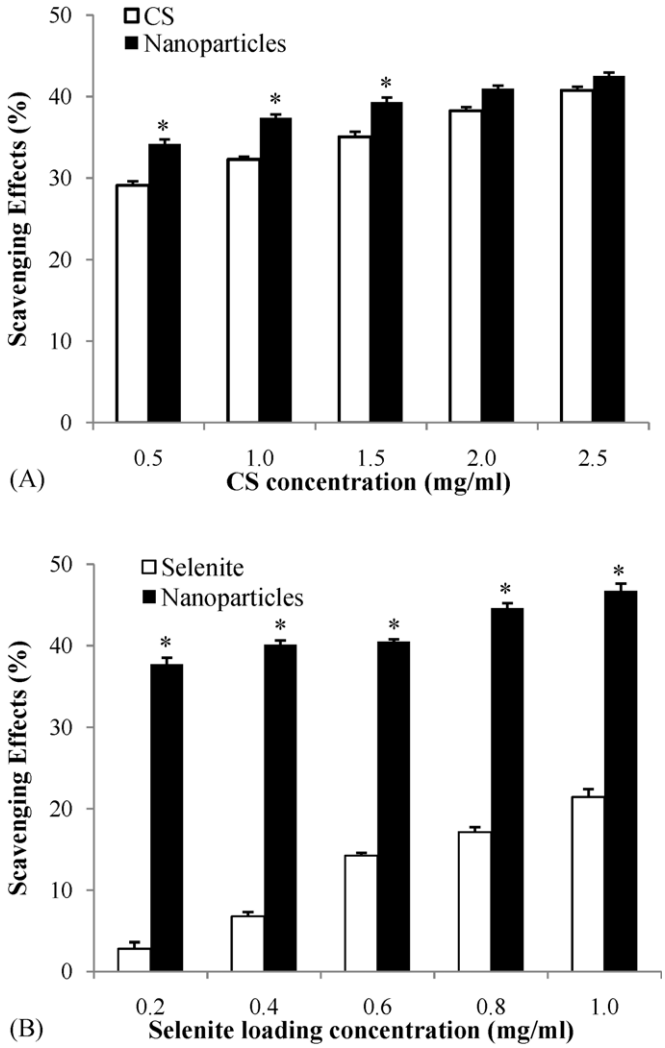

Fig. 6. (A) Effect of CS concentrations on scavenging effect of selenite-loaded CS/TPP nanoparticles against hydroxyl radicals (selenite loading concentration = 0.6 mg/ml, CS-TPP mass ratio = 5:1). (B) Effects of selenite loading concentrations on scavenging effect of nanoparticles against hydroxyl radicals (CS concentration = 1.5 mg/ml, CS-TPP mass ratio = 5:1). Values were expressed as mean ± standard error. *$P < 0.05$, compared with CS (A) or selenite (B) at the equivalent concentration.

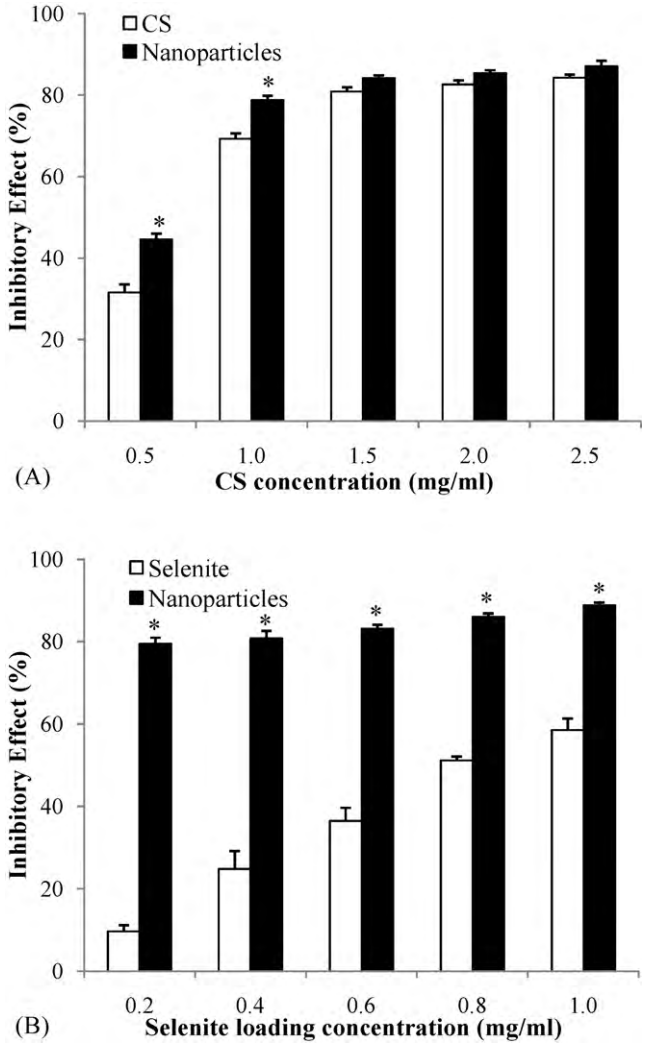

Fig. 7. (A) Effect of CS concentrations on inhibitory effect of selenite-loaded CS/TPP nanoparticles against lipid peroxidation (selenite loading concentration = 0.6 mg/ml, CS-TPP mass ratio = 5:1). (B) Effects of selenite loading concentrations on inhibitory effect of selenite-loaded CS/TPP nanoparticles against lipid peroxidation (CS concentration = 1.5 mg/ml, CS-TPP mass ratio = 5:1). Values were expressed as mean ± standard error. *$P < 0.05$, compared with pure ingredient at the equivalent concentration.

nanoparticles was 2–13 times greater than that of sodium selenite at the equivalent selenite concentrations ($P < 0.05$).

3.6.2. *Inhibitory effect against lipid peroxidation (IEALP)*

The inhibitory effect of selenite-loaded nanoparticles, CS and selenite against lipid peroxidation in linoleic acid system were presented in Fig. 7. CS possessed higher IEALP in higher concentrations, while that selenite-loaded nanoparticles had a similar trend on IEALP which increased from 44% to 87% with increase of CS concentration in formulations (Fig. 7A). No significant difference was observed between IEALP of CS and that of nanoparticles at higher CS concentration. The IEALP of nanoparticles slightly increased from 79% to 88% as the selenite loading concentration increased from 0.2 to 1.0 mg/ml. The IEALP of nanoparticles were significantly improved ($P < 0.05$), compared with selenite at equivalent concentrations (Fig. 7B). Although the IEALP of selenite was stronger at higher concentration reaching 58% at 1.0 mg/ml, when considering the decreased encapsulation efficiency of selenite (45%) at 1.0 mg/ml (Fig. 4B), the increase of selenite loading concentration would not efficiently enhance the antioxidant activities of nanoparticles.

It was reported that when the gold nanoparticles were prepared using CS as a stabilizer, the catalytic activity of gold nanoparticles upon elimination of hydroxyl radicals was remarkably elevated, which was 80-fold higher than that of nanoparticles stabilized by an ascorbic acid (Esumi, Takei, & Yoshimura, 2003). Recently, fungal CS and crab CS have been discovered to possess potent antioxidant properties, including scavenging ability on hydroxyl radicals and inhibitory effect against linoleic acid oxidation (Yen, Yang, & Mau, 2007, 2008). Based on our results, it is suggested that although both selenite and CS contributed to the antioxidant properties of the nanoparticles, the contribution of CS was much greater than that of selenite. The encapsulation of selenite into CS nanoparticles could significantly improve the antioxidant profile of selenite supplementation *in vitro*; however, the *in vivo* evaluation of selenite-loaded CS nanoparticles deserves further studies (on going research).

3.7. *Improved nanoparticle formulations with zein coating*

Studies have shown that a large portion of dietary supplements of selenite cannot be effectively absorbed because of short reten-

Table 2
Effects of zein coating on physicochemical properties of selenite-loaded CS/TPP nanoparticles.

Formulations	Particle size (nm)	PDI	EE (%)	Stimulated GI tract release (%)	
				SGF (2 h)	SIF (4 h)
Without zein coating	233.05 ± 9.86[a]	0.18 ± 0.03	63.34 ± 2.54[a]	93.37 ± 2.25[a]	
Coated with zein (CS to Zein 1:1)	236.93 ± 22.14[a]	0.21 ± 0.06	96.16 ± 3.80[b]	49.06 ± 4.35[b]	50.43 ± 5.72
Coated with zein (CS to Zein 1:3)	454.13 ± 21.15[b]	0.28 ± 0.06	95.71 ± 2.10[b]	45.94 ± 3.33[b]	53. 39 ± 4.47

Note: The selenite-loaded CS/TPP nanoparticles without zein coating: CS concentration, 1.5 mg/ml; selenite loading concentration, 0.6 mg/ml; CS-TPP mass ratio, 5:1. EE, encapsulation efficiency; SGF, simulated gastric fluid; SIF, simulated intestinal fluid. Values were expressed as mean ± standard error. The values with different letter in the same column were significantly different at $P < 0.05$.

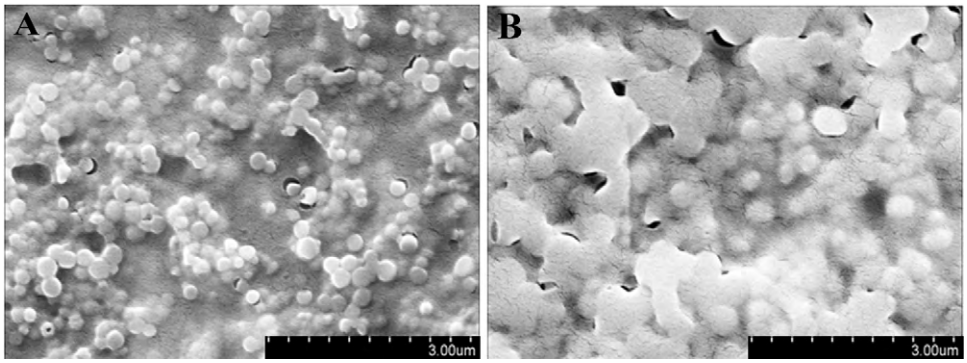

Fig. 8. Scanning electron microscopy (SEM) photographs of zein-coated selenite-loaded CS/TPP nanoparticles. (A) CS:zein = 1:1; (B) CS:zein = 1:3.

tion time in gastrointestinal tract (Dael et al., 2001; Zachara et al., 2006). Considering that selenite is best absorbed in intestine for further utilization in the body, selenite needs to be protected in the encapsulated nanoparticles until it reaches the target site, the intestine. However, from Section 3.5, all formulations of selenite-loaded CS/TPP nanoparticles had fast release effect in PBS and the selenite contents dropped to ~10% within 4 h (Fig. 5). Zein, the prolamine of corn, is a GRAS (generally recognized as safe) component with specific interesting properties, such as self-assembled nanoscale-sized structure, water resistance and film-forming properties. Zein has been widely used in the pharmacuetical and food science area to coat capsules, encapsulate nutrients, provide controlled release, etc. (Shukla & Cheryan, 2001). In our study, it was proposed as a hydrophobic coating material for the prepared nanoparticles and it could be considered as water barrier to inhibit CS swelling and strengthen the polymer matrix through hydrogen bond with CS.

As shown in Table 2, after coating with zein, the encapsulation efficiency of selenite was significantly improved from 60% to 95%. Particle size of zein-coated nanoparticles increased with zein concentration, and reached 450 nm when the mass ratio of CS to zein was 1:3. Interestingly, as the mass ratio of CS to zein was 1:1, the particle size of coated nanoparticles maintained around 260 nm, similar to that of the uncoated nanoparticles, whereas the encapsulation efficiency achieved 96%. Thus, nanoparticles with mass ratio of CS to zein as 1:1 might be the optimal formulation to obtain both small particle size and high encapsulation efficiency. Zein has been proved to possess film-forming ability when treated in acidic system (Wang, Yin, & Padua, 2008), including acetic acid (Shi, Kokini, & Huang, 2009) which was used as a common medium to prepare CS/TPP nanoparticles. In our study, zein can form a coating film around the nanoparticles (Fig. 8A and B), and with higher concentration of zein, the coating was denser and thicker, resulting in increased diameter tested by DLS.

The release profile of zein-coated nanoparticles in PBS medium was illustrated in Fig. 9. Comparing to selenite-loaded CS/TPP nanoparticles without coating, both the burst effect and accumulative release were greatly improved. Burst effect for the coated nanoparticles occurred at 30 min and only 20% of encapsulated selenite released from matrix, while burst effect for the non-coated nanoparticles occurred at 60 min and more than 85% of selenite released out. The accumulative release of selenite within 4 h decreased dramatically from 98% for non-coated nanoparticles to 32% for coated ones. To further investigate the protective effect of zein coating on selenite release, the release profile was examined under simulated gastric fluid (SGF) and simulated intestinal fluid (SIF) digestion conditions with the presence of enzymes (pepsin and pancreatin, respectively). Table 2 showed the selenite encapsulated in CS/TPP nanoparticles without zein coating almost completely released in SGF (93.37 ± 2.25%) in 2 h. However, after coated with zein, the selenite release was greatly prolonged and nanoparticles was well protected against gastric condition,

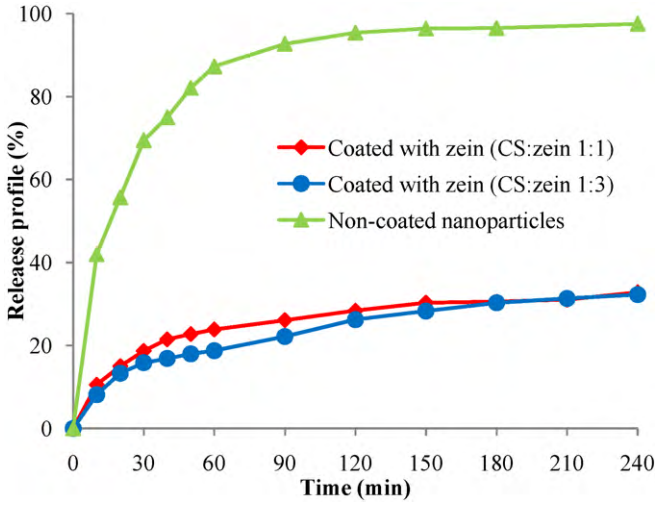

Fig. 9. Effects of zein coating on selenite release profile from nanoparticles. CS concentration = 1.5 mg/ml, selenite loading concentration = 0.6 mg/ml, CS-TPP mass ratio = 5:1. Values were expressed as mean ± standard error. The values with different letter were significantly different at $P < 0.05$.

showing that only about 50% of encapsulated selenite released in SGF. The release of the remaining selenite completed after 4 h of incubation in SIF for both coated samples. No significant difference was observed between the two experimented concentrations of zein coating. Coating the particles with another polymer has been proposed as an effective approach to prolong the controlled release of encapsulated nutraceuticals. Somchue et al. (2009) found after α-tocopherol encapsulated protein-based delivery particles were coated with alginate, the release profile of delivery was retarded prominently. From our study, the release of selenite as well as encapsulation efficiency of CS/TPP nanoparticles was dramatically improved by zein coatings.

4. Conclusion

The present study demonstrated that selenite-loaded CS/TPP nanoparticles can be successfully prepared under mild conditions via ionic gelation method. Physicochemical properties, such as particle size, surface charge, encapsulation efficiency, and controlled release can be modulated by controlling critical fabricating parameters including the CS and selenite loading concentrations. The encapsulation of selenite into CS can significantly improve the *in vitro* antioxidant properties, compared with free selenite. After coated with zein, the encapsulation efficiency was greatly increased and release profile was dramatically retarded, indicating that zein-coated selenite-CS/TPP nanoparticles possess a high potential to be developed as an alternative to traditional selenium treatment or supplementation. Moreover, the i*n vitro* cytotoxicity evaluation of selenite encapsulated nanoparticle formulations are being studied in Dr. Cheng's Lab, which would give further information on cellular Se retention, toxicity as well as DNA response of selenite-loaded CS/TPP nanoparticles (data will be submitted for publication).

Acknowledgement

This work is partially supported by Hatch fund of USDA. We acknowledge the support of the Maryland NanoCenter.

References

Björkhem-Bergman, L., Jönsson, K., Eriksson, L. C., Olsson, J. M., Lehman, S., Paul, C., et al. (2002). Drug-resistant human lung cancer cells are more sensitive to selenium cytotoxicity: Effects on thioredoxin reductase and glutathione reductase. *Biochemical Pharmacology*, *63*, 1875–1884.

Cheng, W. H. (2009). Impact of inorganic nutrients on maintenance of genomic stability. *Environmental and Molecular Mutagenesis*, *50*, 349–360.

Dael, P. V., Davidsson, L., Munoz-Box, R., Fay, L. B., & Barclay, D. (2001). Selenium absorption and retention from a selenite- or selenate-fortified milk-based formula in men measured by a stable-isotope technique. *British Journal of Nutrition*, *85*, 157–163.

Desai, M. P., Labhasetwar, V., Amidon, G. L., & Levy, R. J. (1996). Gastrointestinal uptake of biodegradable microparticles: Effect of particle size. *Pharmaceutical Research*, *13*(12), 1838–1845.

Desai, M. P., Labhasetwar, V., Walter, E., Levy, R. J., & Amidon, G. L. (1997). The mechanism of uptake of biodegradable microparticles in Caco-2 cells is size dependent. *Pharmaceutical Research*, *14*(11), 1568–1573.

Dudhani, A. R., & Kosaraju, S. L. (2010). Bioadhesive chitosan nanoparticles: Preparation and characterization. *Carbohydrate Polymers*, *81*, 243–251.

Dung, T. H., Lee, S. R., Han, S. D., Kim, S. J., Ju, Y. M., Kim, M. S., et al. (2007). Chitosan-TPP nanoparticle as a release system of antisense oligonucleotide in the oral environment. *Journal of Nanoscience and Nanotechnology*, *7*(11), 3695–3699.

Esumi, K., Takei, N., & Yoshimura, T. (2003). Antioxidant-potentiality of gold-chitosan nanocomposites. *Colloids and Surfaces B: Biointerfaces*, *32*, 117–123.

Ferguson, L. R., Philpott, M., & Karunasinghe, N. (2006). Oxidative DNA damage and repair: Significance and biomarkers. *Journal of Nutrition*, *136*, 2687S–2689S.

Gan, Q., & Wang, T. (2007). Chitosan nanoparticle as protein delivery carrier-systematic examination of fabrication conditions for efficient loading and release. *Colloids and Surfaces B: Biointerfaces*, *59*, 24–34.

Gan, Q., Wang, T., Cochrane, C., & McCarron, P. (2005). Modulation of surface charge, particle size and morphological properties of chitosan-TPP nanoparticles intended for gene delivery. *Colloids and Surfaces B: Biointerfaces*, *44*, 65–73.

Grenha, A., Seijo, B., & Remuñán-López, C. (2005). Microencapsulated chitosan nanoparticles for lung protein delivery. *European Journal of Pharmaceutical Science*, *25*, 427–437.

Hu, B., Pan, C. L., Hou, Z. Y., Ye, H., Hu, B., & Zeng, X. X. (2008). Optimization of fabrication parameters to produce chitosan-tripolyphosphate nanoparticles for delivery of tea catechins. *Journal of Agricultural and Food Chemistry*, *56*, 7451–7458.

Khlifi, S., El Hachimi, Y., Khalil, A., Es-Safi, N., & El Abbouyi, A. (2005). In vitro antioxidant effect of *Globularia alypum* L. hydromethanolic extract. *Indian Journal of Pharmacology*, *37*(4), 227–237.

Ko, J. A., Park, H. J., Hwang, S. J., Park, J. B., & Lee, J. S. (2002). Preparation and characterization of chitosan microparticles intended for controlled drug delivery. *International Journal of Pharmacology*, *249*, 165–174.

Kockisch, S., Ress, G. D., Young, S. A., Tsibouklis, J., & Smart, J. D. (2003). Polymeric microspheres for drug delivery to the oral cavity: An *in vitro* evaluation of mucoadhesive potential. *Journal of Pharmaceutical Science*, *92*(8), 1614–1623.

Lawrie, G., Keen, I., Drew, B., Chandler-Temple, A., Rintoul, L., Fredericks, P., et al. (2007). Interactions between alginate and chitosan biopolymers characterized using FTIR and XPS. *Biomacromolecules*, *8*, 2533–2541.

Liu, A., Song, W., Cao, D., Liu, X., & Jia, Y. (2008). Growth inhibition and apoptosis of human leukemia K562 cells induced by seleno-short-chain chitosan. *Methods and Findings Experimental and Clinical Pharmacology*, *30*(3), 181–186.

Moak, M. A., & Christensen, M. J. (2001). Promotion of lipid oxidation by selenate and selenite and indicators of lipid peroxidation in the rat. *Biological Trace Element Research*, *79*, 257–269.

Navas-Acien, A., Bleys, J., & Guallar, E. (2008). Seleniumintake and cardiovascular risk: What is new? *Current Opinion Lipidology*, *19*, 43–49.

Navarro-Alarcon, M., & Cabrera-Vique, C. (2008). Selenium in food and the human body: A review. *Science of the Total Environment.*, *400*, 115–141.

Picker-Freyer, K. M., & Brink, D. (2006). Evaluation of powder and tableting properties of chitosan. *AAPS PharmSciTech*, *7*, E1–E10.

Qin, C. Q., Xiao, L., Du, Y. M., & Gao, X. H. (2002). Antitumor activity of chitosan hydrogen selenites. *Chinese Chemical Letter*, *13*(3), 213–214.

Ray, A. L., Semba, R. D., Walston, J., Ferrucci, L., Cappola, A. R., Ricks, M. O., et al. (2006). Low serum selenium and total carotenoids predict mortality among older women living in the community: The women's health and aging studies. *Journal of Nutrition*, *136*, 172–176.

Shah, S., Pal, A., Kaushik, V. K., & Devi, S. (2009). Preparation and characterization of venlaxine hydrochloride-loaded chitosan nanoparticles and *in vitro* release of drug. *Journal of Applied Polymer Science*, *112*, 2876–2887.

Shimizu, R., Ueno, H., Okuno, T., Sakazaki, F., & Nakamuro, K. (2009). Effect of sodium selenite supplementation on glucose intolerance and pancreatic oxidative stress in type 2 diabetic mice under different selenium status. *Journal of Health Science*, *55*, 271–280.

Shimoda, J., Onishi, H., & Machida, Y. (2001). Bioadhesive characteristics of chitosan microspheres to the mucosa of rat small intestine. *Drug Development and Industrial Pharmacy*, *27*(6), 567–576.

Shukla, R., & Cheryan, M. (2001). Zein: The industrial protein from corn. *Industrial Crops and Products*, *13*(3), 171–192.

Sinha, V. R., Singla, A. K., Wadlhawan, S., Kaushik, R., & Kumria, R. (2004). Chitosan microspheres as a potential carrier for drugs. *International Journal of Pharmaceutics*, *274*, 1–33.

Shi, K., Kokini, J. L., & Huang, Q. (2009). Engineering zein films with controlled surface morphology and hydrophilicity. *Journal of Agricultural and Food Chemistry*, *57*(6), 2186–2192.

Somchue, W., Sermsri, W., Shiowatana, J., & Siripinyanond, A. (2009). Encapsulation of α-tocopherol in protein-based delivery particles. *Food Research International*, *42*, 909–914.

Tian, F., Li, B., Ji, B. P., Yang, J. H., Zhang, G. Z., Chen, Y., et al. (2009). Antioxidant and antimicrobial activities of consecutive extracts from *Galla chinensis*: The polarity affects the bioactivities. *Food Chemistry*, *113*, 173–179.

Thomson, C. D. (2004). Assessment of requirements for selenium and adequacy of selenium status: A review. *European Journal of Clinical Nutrition*, *58*, 391–402.

Veiga, N., Rivero-Huguet, M., & Huertas, R. (2008). An improved spectrofluorometric determination of selenium in biological materials after microwave digestion. *Atomic Spectroscopy*, *29*(2), 63–68.

Wang, Q., Yin, L., & Padua, G. W. (2008). Effect of hydrophilic and lipophilic compounds on zein microstructures. *Food Biophysics*, *3*, 174–181.

Wang, S. L., Yao, H. H., Guo, L. L., Dong, L., Li, S. G., Gu, Y. P., et al. (2009). Selection of optimal sites for TGFB1 gene silencing by chitosan-TPP nanoparticle-mediated delivery of shRNA. *Cancer Genetics and Cytogenetics*, *190*, 8–14.

Wu, Y., Yang, W. L., Wang, C. C., Hu, J. H., & Fu, S. K. (2005). Chitosan nanoparticles as a novel delivery system for ammonium glycyrrhizinate. *International Journal of Pharmacology*, *295*, 235–245.

Xiang, N., Zhao, R., & Zhong, W. X. (2009). Sodium selenite induces apoptosis by generation of superoxide via the mitochondrial-dependent pathway in human prostate cancer cells. *Cancer Chemotherapy and Pharmacology*, *63*, 351–362.

Yang, R., Yang, S. G., Shim, W. S., Cui, F., Cheng, G., Kim, I. W., et al. (2009). Lung-specific delivery of paclitaxel by chitosan-modified PLGA nanoparticles via transient formation of microaggregates. *Journal of Pharmaceutical Science*, *98*(3), 970–984.

Yen, M. T., Yang, J. H., & Mau, J. L. (2007). Antioxidant properties of fungal chitosan from shiitake stipes. *LWT-Food Science and Technology*, *40*, 225–261.

Yen, M. T., Yang, J. H., & Mau, J. L. (2008). Antioxidant properties of chitosan from crab shells. *Carbohydrate Polymer*, *74*, 840–844.
Zachara, B. A., Gromadzinska, J., Wasowizc, W., & Zbrog, Z. (2006). Red blood cell and plasma peroxidase activities and selenium concentration in patients with chronic kidney disease: A review. *Acta Biochimca Polonica*, *53*(4), 663–677.
Zhang, Y. Y., Yang, Y., Tang, K., Hu, X., & Zou, G. L. (2008). Physicochemical characterization and antioxidant activity of quercetin-loaded chitosan nanoparticles. *Journal of Applied Polymer Science*, *107*, 891–897.
Zhou, S. B., Deng, X. M., & Li, X. H. (2001). Investigation on a novel core-coated microspheres protein delivery system. *Journal of Controlled Release*, *75*, 27–36.